Chapter 2
Rietveld Refinement

Peter W. Stephens

Abstract Rietveld refinement is generally the last stage of structure determination. The determination of unknown structures generally proceeds through a series of hypotheses of lattice, space group, atomic structure, each of which is subject to subsequent verification, so Rietveld refinement is the final test of the correctness of a structure. Unfortunately, there are not such clear tests of the veracity of a Rietveld refinement as there are of single crystal structures, and so a clear understanding of the process is required to judge a correct solution. This chapter will not directly address another frequent use of the technique, quantitative phase analysis, although many of the principles discussed here are relevant. There are any number of widely used programs and this chapter emphasizes the general features of the process over specific implementations.

2.1 Introduction

In powder diffraction, unlike a single crystal experiment, the 3D diffraction pattern is compressed into one dimension. While each (*hkl*) diffraction peak occupies a specific position, the density of peaks rapidly rises with increasing diffraction angle 2θ (or decreasing time of flight in a pulsed neutron experiment) that most peaks are overlapped, and it is a non-trivial task to separate their intensities.[1] A nice example of a pre-Rietveld structure determination from powder x-ray data

[1]For notational convenience I will restrict this discussion to angle-dispersive experiments, with absolutely no prejudice against pulsed neutron techniques.

P.W. Stephens (✉)
Department of Physics and Astronomy, State University of New York (SUNY), Stony Brook, NY 11776, USA
e-mail: pstephens@notes.cc.sunysb.edu

U. Kolb et al. (eds.), *Uniting Electron Crystallography and Powder Diffraction*,
NATO Science for Peace and Security Series B: Physics and Biophysics,
DOI 10.1007/978-94-007-5580-2_2,

is Zachariasen's (1951) solution of cubic Pu_2C_3 [1]. The structure was solved by determining the intensity of a set of diffraction peaks, and then choosing space group and coordinate(s) to fit. This works well for reasonably high symmetry, for relatively simple structures (only the Pu atom was considered in matching intensities, and the number and location of C atoms was inferred), and for people as ingenious as Zachariasen.

The Rietveld method, in use since 1969, goes the other direction [2]. From a hypothesized structure, one calculates the diffraction pattern to compare with the measured diffraction profile, i.e., intensity as a function of 2θ in a step scan. That allows a treatment of overlapping peaks which, we will see, allows the maximum amount of information to be extracted from an experimental pattern. This was originally done for relatively low resolution CW neutron data from a reactor, for which it was possible to give a fairly accurate model lineshape. In general, one imagines that the lineshape, which depends on a convolution of instrumental parameters and sample microstructure, can be specified more or less independently of the crystal structure (peak positions and intensities), so that a simultaneous refinement of lineshape and structure can be factored into reliable information about each, separately. We will return to this point subsequently.

For the purpose of this discussion, we assume that an approximate structural model (lattice parameters, space group, atom positions) is at hand. Our task is to optimize those various parameters, while keeping a close watch for any symptoms that the starting point was incorrect and needs to be revisited. The information in a powder diffraction pattern consists of:

- Peak positions, which depend on lattice dimensions and space group,
- Peak intensities, which depend on the distribution of atoms within the unit cell,
- Peak shapes, which are a convolution of instrumental parameters and the microstructure of the sample.

Crystallographic structure starts with the unit cell, defined by translation vectors $\boldsymbol{a}$, $\boldsymbol{b}$, $\boldsymbol{c}$. Diffraction peaks form a reciprocal lattice spanned by vectors $\boldsymbol{a}^*$, $\boldsymbol{b}^*$, $\boldsymbol{c}^*$ such that any diffraction peak can be specified as $\boldsymbol{Q} = h\boldsymbol{a}^* + k\boldsymbol{b}^* + l\boldsymbol{c}^*$, defined as $\boldsymbol{a}^* = 2\pi(\boldsymbol{b} \times \boldsymbol{c})/\boldsymbol{a}\cdot(\boldsymbol{b} \times \boldsymbol{c})$, *etc*. The diffracting planes for each reflection are separated by $d = 2\pi/|\boldsymbol{Q}|$, and the diffraction condition that the vector difference between incident and diffracted radiation wave vectors $\boldsymbol{k_i}$ and $\boldsymbol{k_f}$ (of equal magnitude $2\pi/\lambda$) is $\boldsymbol{Q} = \boldsymbol{k_f} - \boldsymbol{k_i}$ is equivalent to Bragg's law, $\lambda = 2d\sin\theta$. The above definitions are those commonly used in the physics community; others frequently drop all of the factors of 2π in the equations and definitions in the foregoing paragraph. The position of a peak in a powder pattern can be obtained from the magnitude of $\boldsymbol{Q}$, while the equations above can be put in the convenient form

$$\sin^2\theta = \left(\lambda^2/4d^2\right) = \left(\lambda^2/4\right)\left(Ah^2 + Bk^2 + Cl^2 + Dkl + Ehl + Fhk\right),$$

where the metric parameters $A, \ldots, F$ depend only on the real (or reciprocal) lattice parameters.

In a powder pattern, the integrated intensity of a given peak is

$$I(hkl) = cM_{hkl}\left|\sum_{\text{atoms } j} f_j \exp 2\pi i\,[hx + ky + lz]\ \exp -2W\right|^2 \text{g}LP(\theta)$$

Here c is an overall scale factor, M_{hkl} is the multiplicity of the given peak, LP is the Lorentz-Polarization factor, *e.g.*, $LP(\theta) = 1/(\sin\theta \sin 2\theta)$ for x-rays polarized perpendicular to the scattering plane and a detector scanning 2θ with constant solid angle. f_j is the atomic scattering factor of the jth atom, including consideration of partial or mixed occupancy, and $\exp -2\,W$ is the Debye-Waller factor. The sum runs over all atoms in the unit cell, including symmetry equivalent positions generated by the space group. Details of the derivation and implementation of this equation are given in any comprehensive crystallography text, e.g., Giacovazzo [3].

2.2 Lineshape

In order to obtain a computed powder pattern, $Y^{calc}(2\theta)$, one must model the peak shape, taking into account contributions both of the sample microstructure and the diffractometer. Treatment of all of these effects is well beyond the scope of this paper, but we can briefly summarize the usual approach to Rietveld refinement. The comprehensive text edited by Dinnebier and Billinge contains much more detail [4].

Consider the case of an ideal lattice, truncated to spherical shape. Figure 2.1 shows the powder-averaged lineshape, computed from the Debye equation, for a sphere with a diameter of 100 lattice spacings. The full width at half maximum of this peak is $\Gamma = 0.011 \times 2\pi/a$ in Q.

The Scherrer equation, $\text{L} = \text{K}\lambda/\Gamma_{2\theta}\cos\theta$, is frequently used to estimate crystallite size L, where K is a numerical constant having something to do with the (assumed) shape of the grains and $\Gamma_{2\theta}$ is the diffraction peak FWHM in radians. The numerical computation that led to Fig. 2.1 gives $\text{K} \approx 1.10$ for a particle of spherical shape. Powder samples with a single grain size are rare in practice; a distribution of grain sizes will wash out the observed peak shape function and further obscure the relationship between peak width and grain size. For almost all Rietveld refinements of crystal structures, the microstructural details that could be extracted from the lineshape are secondary to the desire to have a simple analytical model, and so one can imagine that the ideal lineshape function might be modeled as a Gaussian or Lorentzian. Figure 2.1 shows Gaussian and Lorentzian lineshapes of the same full width at half maximum, from which it is obvious that the one has tails that are too weak, and the other, too strong. It is generally satisfactory to use an interpolation of the two, for example, a pseudo-Voigt centered at $2\theta_0$,

$$f(2\theta) = \eta\frac{\Gamma/4\pi}{(2\theta - 2\theta_0)^2 + \Gamma^2/4} + (1-\eta)\frac{\sqrt{4\ln 2}}{\Gamma\sqrt{\pi}}\exp -\left(\frac{(2\theta - 2\theta_0)^2}{\Gamma^2}4\ln 2\right)$$

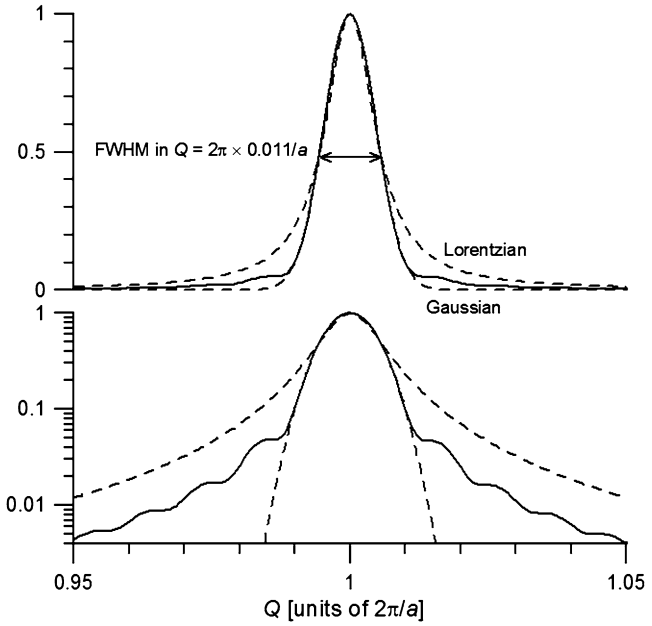

Fig. 2.1 Computed powder lineshape of the (100) peak of a spherical grain, 100 atoms in diameter

normalized to unit integrated intensity, with full width at half maximum Γ, and interpolation parameter η.

Another sample dependent effect frequently encountered is microstrain, whereby the peak width in Q is proportional to the diffraction order, *i.e.*, the width in 2θ grows in proportion to $\tan\theta$. One could rationalize that effect by imagining that some form of disorder causes each crystallite to have a slightly different lattice parameter. A more microscopically satisfying description would come from considering the internal strains within each individual crystallite caused by lattice defects, and then computing the diffraction pattern so produced. However, this requires a lot more effort than is usually justified for a crystal structure analysis.

Especially in high resolution measurements, it is frequently found that fitting experimental lineshapes require more elaborate models of size or strain, *e.g.*, to take account of anisotropic broadening; these are available in most Rietveld software, and are beyond the scope of the current treatment. Combining the effects of size and strain, and imagining that contributions to the width of a diffraction peak can be modeled as a convolution, it is plausible that the observed width in diffraction angle 2θ could be written as $\Gamma_{2\theta} = X/\cos\theta + Y\tan\theta$, where X and Y are parameters that represent the size and strain contributions. (This expression is justified if both contributions are regarded as Lorentzians, whose widths add directly in convolution. For Gaussians, the widths would add in quadrature).

The first application of the Rietveld method was to powder neutron diffraction at a CW source, where the instrumental lineshape is essentially a Gaussian whose

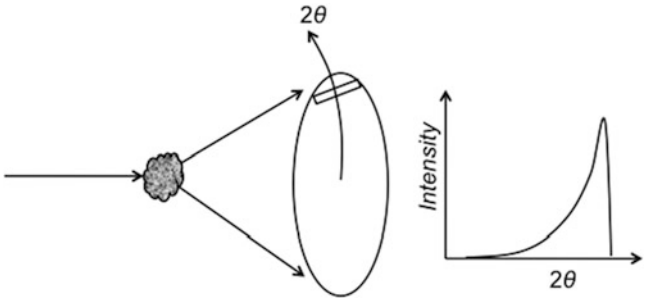

Fig. 2.2 Sketch illustrating the origin of low-angle tails on diffraction peaks due to axial divergence

variance depends on the diffraction angle as $\sigma^2 = U\tan^2\theta + V\tan\theta + W$, where the parameters U, V, and W depend on the width of the collimators, and d-spacings and mosaics of the monochromator [5]. X-ray spectral lines are combinations of several Lorentzians in wavelength, and in high resolution diffractometers with perfect crystals as monochromators and/or analyzers, the intrinsic reflection curves have long ($\Delta\theta^{-2}$) tails. The approach of convoluting the contribution of each optical element, known as fundamental parameters, was described in detail by Klug and Alexander [6]. The utility of fundamental parameters approach has greatly expanded with modern computational techniques, exemplified by Cheary and Coelho [7]. While such methods are extremely powerful, they are generally beyond the scope of this chapter, and so we will restrict our attention to the more widely used empirical lineshape models.

One important aberration in most powder diffractometers is axial divergence. This produces asymmetric peaks, especially at low diffraction angles. The effect may be visualized as shown in Fig. 2.2, where the diffracted radiation from a given order radiates from the sample as a cone. The edges of the detector slit intercept part of that cone below the nominal diffraction angle, and so there is a tail extending to the low angle side of the peak, which is especially pronounced for low diffraction angles. Several analytical treatments of this effect have been published, and it is incorporated in modern Rietveld programs. In the opinion of this author, unsubstantiated numerical approaches to this effect, such as the split-Pearson VII lineshape, should be avoided.

A good point of reference is the lineshape function used in GSAS [8], which is an approximate (pseudo-Voigt) convolution of a Gaussian with variance $\sigma^2 = U\tan^2\theta + V\tan\theta + W + P/\cos^2\theta$ with a Lorentzian of full width at half maximum (FWHM) $\Gamma = X/\cos\theta + Y\tan\theta$ and an asymmetric function to describe axial divergence of the diffracted beam. The origin of these parameters can be traced to elements of the discussion above, although it is not at all clear how to unravel information about sample microstructure from their converged values. Rietveld codes usually incorporate other parameters for instrumental corrections such as detector offset angle, sample displacement, etc.

Since the purpose of Rietveld refinement is to adjust various structural and lineshape parameters to obtain the best agreement between model and data, it is important to be clear on the figure of merit used. Suppose that the data consists of x-ray intensities collected in a step scan of 2θ, so that the observed intensity and standard error at each point are $Y^{obs}(2\theta)$ and $\sigma_{2\theta}$ respectively. (Here we are regarding 2θ as an index spanning the discrete set of measured data points). If $Y^{obs}(2\theta)$ is the number of counts detected, $\sigma_{2\theta}$ is simply $(Y^{obs}(2\theta))^{1/2}$, but it is frequently the case that the intensity is not constant through the scan, *e.g.*, for a synchrotron or pulsed neutron source, or if a variable counting time data collection strategy is in use. In that case, $Y^{obs}(2\theta)$ must be normalized to the dose of radiation reaching the sample while the data point at 2θ was being integrated, and $\sigma_{2\theta}$ scaled by the same factor. If the computed profile is given by $Y^{calc}(2\theta)$, the familiar reduced χ^2 parameter is given by

$$\chi^2 = (N-P)^{-1}\sum_{2\theta}^{N}\left(\frac{Y^{obs}(2\theta)-Y^{calc}(2\theta)}{\sigma_{2\theta}}\right)^2,$$

where N is the number of points in the data set and P is the number of parameters adjusted in the fit. If the deviation between model and observed data is due to the counting statistics alone, one expects χ^2 to be very close to unity. Another parameter frequently used is the weighted profile R-factor, defined as

$$R_{wp} = \sum_{2\theta}\left(\frac{Y^{obs}(2\theta)-Y^{calc}(2\theta)}{\sigma_{2\theta}}\right)^2 \Bigg/ \sum_{2\theta}\left(\frac{Y^{obs}(2\theta)}{\sigma_{2\theta}}\right)^2$$

Again, if differences between model and data are purely due to counting statistics, R_{wp} should approach the expected R-factor, R_{exp}, which is given by

$$R_{exp} = (N-P)\Bigg/\sum_{2\theta}\left(\frac{Y^{obs}(2\theta)}{\sigma_{2\theta}}\right)^2$$

It is evident that $R_{wp}/R_{exp} = \sqrt{\chi^2}$, a number which is also referred to as the "goodness of fit" (GOF).

An obvious question is whether there is some threshold χ^2 or R_{wp} which indicates a correct solution. The answer is no, and this is a source of consternation to people who try to publish refinements, as well as journal editors and referees, who are usually used to the clearer diagnostic signatures of a valid structure from single crystal data. Indeed, in comparing two different Rietveld refinements, even of the same sample, it is not necessarily the case that a better figure of merit indicates superior structural results. This arises partly because the quality of a Rietveld fit depends on details of the data that have little to do with the structure, and partly

because most of the information content in a diffraction pattern is at the higher angles where peaks are generally weaker and more strongly overlapped, but likely have less effect on the refinement statistics than a few strong low angle peaks. For this reason, it is recommended to spend more data collection time on the high angle peaks for the refinement of any complicated material. These issues are discussed in greater detail in several useful papers, *e.g.*, references [9] and [10].

In refining a structure, one must be prepared to examine both the fit and the reasonableness of the result in detail. A paper entitled "Rietveld refinement of a wrong crystal structure" provides a cautionary example, although there are significant danger signals in the example discussed there [11].

2.3 Intensity Estimation and Extraction from Powder Diffraction Pattern

The Rietveld method offers an approximate technique to estimate intensities of partially overlapping peaks from the recorded profile, based in part on the structural model. Imagine that the computed, normalized profile function of the nth diffraction peak is given by $f_n(2\theta)$, so that the computed profile at a given point of the profile is given by

$$Y^{calc}(2\theta) = \sum_{2\theta} I_n \, f_n(2\theta) + B(2\theta)$$

where B is the background function, and I_n is the integrated intensity of the n^{th} diffraction peak. Measured intensity at a given profile point is attributed to all diffraction peaks in proportion to their calculated contribution at that point, i.e.,

$$I_n^{obs} = \sum_{2\theta} \left(Y_i^{obs}(2\theta) - B(2\theta)\right) \frac{I_n^{calc} f_n(2\theta)}{\sum_m I_m^{calc} f_m(2\theta)}$$

One can then compute the standard crystallographic Bragg R factor comparing "observed" and computed intensities,

$$R_B = \sum_n |I_n^{obs} - I_n^{calc}| \Big/ \sum_n I_n^{obs} .$$

Of course, the estimated intensities are obviously biased by the optimistic model-based division of intensity of unresolved peaks.

It is frequently desired to "deconstruct" a powder diffraction profile into a set of integrated intensities of the diffraction peaks present. Armel Le Bail noted

that the Rietveld intensity estimation can be used in an iterative fashion to obtain estimates of the integrated intensities of all peaks in a powder pattern [12]. Cycles of refinement of profile, lattice, and background parameters alternate with reassignments of the set of integrated intensities, and the process is repeated until it converges. Computationally, this is very convenient because most of the work is already performed in the Rietveld program. The method is widely used and has had a tremendous impact on the techniques of structure determination from powder data.

Another method of intensity extraction was pioneered by Pawley, who treated the set of diffraction peak intensities $\{I^{obs}\}$ as parameters in a least squares fit, along side of the profile, lattice, and background parameters [13]. This idea faces the technical obstacle of instability of the refinement when poorly peaks are present. Indeed, the usual Hessian matrix is singular if two peaks have the same position, as occurs, for example, with cubic (333) and (511) reflections. Until relatively recently (~10y), the Pawley method was less used than the Le Bail method, but it is now incorporated into several widely-used Rietveld codes. One direct advantage of the Pawley method is that it provides estimates of the correlation between extracted intensities. This can be used to compare the quality of a structural model much more rapidly than by computing an entire profile R_{wp} [14]. Indeed, it has been shown that no information is lost in reducing a powder diffraction pattern to Pawley intensities and covariance matrix $\boldsymbol{A}$, so that a quality of fit parameter

$$\chi^2 = \sum_{n,m} \left(I_n^{obs} - I_n^{calc}\right)\left(A^{-1}\right)_{nm}\left(I_m^{obs} - I_m^{calc}\right)$$

is just as good as a full pattern Rietveld fit to refine a model (with some subtleties associated with the background) [15]. A similar method has been applied to intensities obtained from a Le Bail fit [16].

Whether the Le Bail or the Pawley method is used, a lineshape fit to an experimental data set is an important intermediate step in determining a crystal structure from powder data. It generally allows accurate refinement of lattice parameters, and a visual inspection can reveal whether a proposed lattice and space group is correct, as well as the presence of impurities. R_{wp} of a Pawley or Le Bail fit can be regarded as the target of a correct structural refinement, insofar as the difference between such a fit and the structural Rietveld refinement lie in the integrated intensities of the diffraction lines.

We now briefly illustrate some of the preceding points by analysis of a sample of Rb_3C_{60} [17]. Figure 2.3a shows the data, collected at a wavelength of 0.69970 Å at beamline X3B1 at the NSLS, in 2002. The experimental conditions were a double crystal Si(111) monochromator and a Ge(111) analyzer, with no focusing optics. The sample was in a 1 mm diameter capillary, spun about its axis to improve the powder statistics. The illuminated area extended about 8 mm along the capillary, and the horizontal (out of scattering plane) slits before the detector were also 8 mm

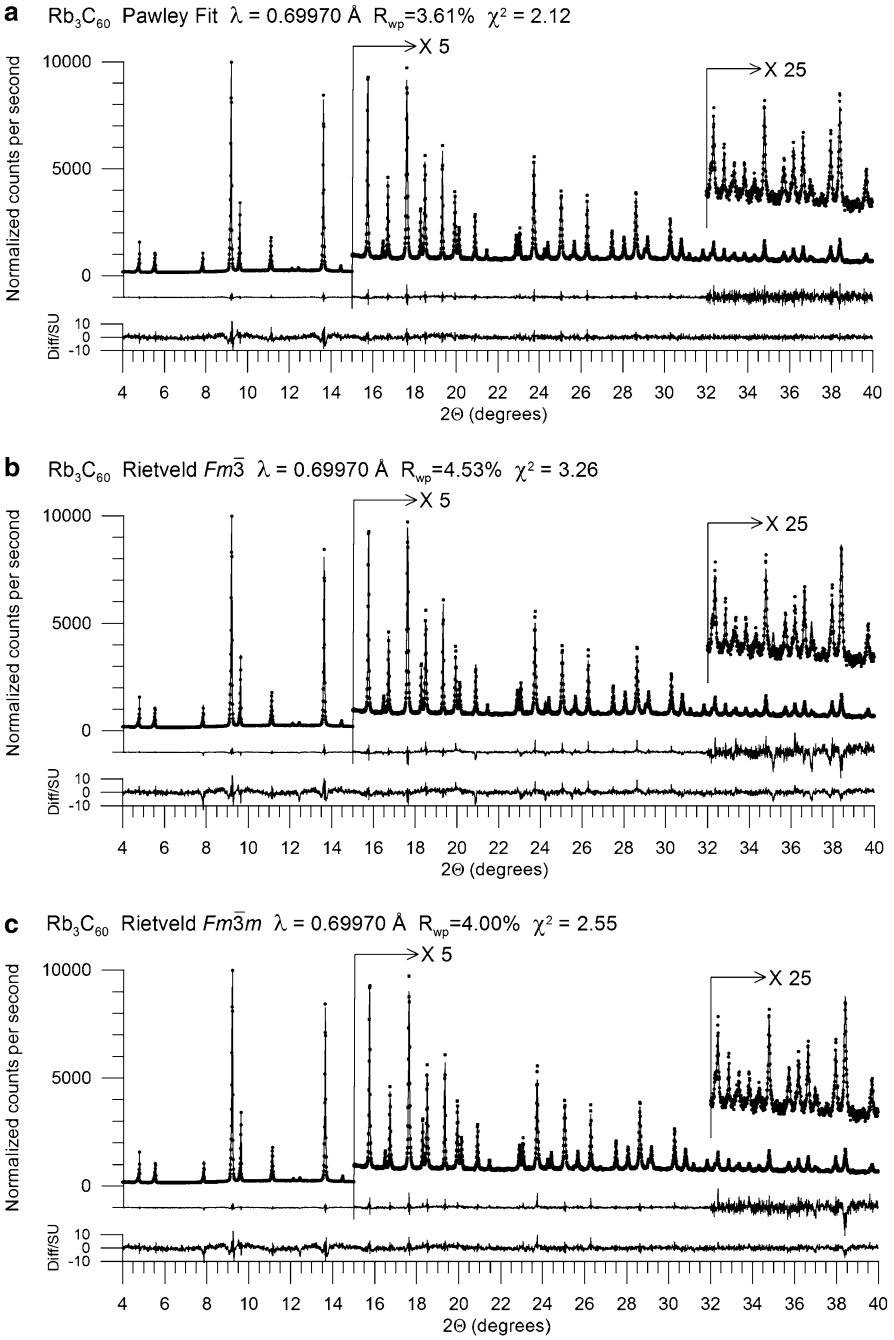

Fig. 2.3 (**a**) Pawley fit to Rb_3C_{60} PXRD data, based on model described in text. Difference curves are shown both in measured intensity (with the same vertical scale changes as the data and model) and as difference divided by the standard uncertainty of each data point (from counting statistics). (**b**) Rietveld refinement in space group $Fm\bar{3}$. (**c**) Rietveld refinement in space group $Fm\bar{3}m$

wide, about 300 mm from the sample. Visual inspection of the data reveals that it has face-centered cubic structure, and shows clearly the aforementioned low angle asymmetry.

Figure 2.3a actually shows a Pawley fit to the data, with axial divergence refined to a value consistent with the known diffractometer geometry, no observable size broadening, and diffraction FWHM proportional to tanθ with roughly equal Gaussian and Lorentzian components. Actually, the strain broadening is slightly anisotropic, with peaks about 30% broader along the {100} directions than along {111}. This can be modeled phenomenologically, and, at least in the case of cubic materials, qualitatively understood as arising from the elastic response to random internal stresses [18]. The background is a quadratic polynomial plus a term in 1/θ, plus a broad (pseudo-Voigt) peak centered at 11.5°. This Pawley fit has Rwp = 3.61%, $\chi^2 = 2.12$, which, frankly, is about as good as it gets.

With the benefit of hindsight, we can immediately solve the structure. The lattice parameter (14.424 Å) is slightly larger than that of an fcc crystal of C_{60}, and a moment's consideration of the cubic close packing of spheres shows that there are two tetrahedral and one octahedral spaces per sphere, which are clearly the sites of the Rb cations, with fractional coordinates (¼, ¼, ¼) and (½, 0, 0) respectively. Examination of a soccer ball leads to the conclusion that it fits naturally into a site of cubic point symmetry, with three-fold axes at the centers of hexagons pointing in the [111] directions, and two-fold axes, at the center of the stitching between two hexagons, pointing in [100] directions. That leads to three crystallographically distinct sites for C atoms: two in general positions (*x, y, z*), and one on the coordinate plane (0*, y, z*). Space group $Fm\bar{3}$ seems the obvious choice, with a multiplicity of 96 in the general position and 48 in the *y*-*z* plane, for a total of 4×60 carbon atoms. Throwing three carbon atoms at random positions, along with the two fixed cations, into a Rietveld program (here, TOPAS, ref. [19]), quickly converges to the decent-looking solution shown in Fig. 2.3b. It was previously noted that even subtle problems in a Rietveld refinement can reveal fundamentally incorrect assumptions. As it happens, Fig. 2.3b is based on an incorrect space group. The fullerene molecule can be rotated by 90° without changing any of the Rb-C distances, which suggests that it could be disordered. Indeed, going to space group $Fm\bar{3}m$ with 50% occupancy of each C position embodies this disorder, and produces the significantly better fit shown in Fig. 2.3c. Despite the small change in refinement statistics, the better fit is clearly evident, especially at high angles. (Note to skeptics – this disorder appears much more clearly in neutron refinements of Rb3C60, as well as in the isostructural K_3C_{60}). The refined bond distances, shown along with refinement statistics in Table 2.1, are also somewhat more plausible in the disordered model. We will stop short of considering further improvements in the model, such as cation vacancies and anisotropic thermal parameters, illustrating the maxim that no Rietveld refinement is ever entirely finished, merely abandoned.

Table 2.1 Refinement statistics and derived bond lengths of Rb_3C_{60} fits shown in Fig. 2.3

	Pawley	$Fm\bar{3}$	$Fm\bar{3}m$
R_{wp} (%)	3.61	4.53	4.00
χ^2	2.12	3.26	2.55
R_B (%)	0.43	2.31	1.26
Double bond (Å)		1.346(5)	1.389(8)
Double bond (Å)		1.347(7)	1.405(6)
Single bond (Å)		1.418(5)	1.442(5)
Single bond (Å)		1.494(5)	1.443(5)
Single bond (Å)		1.504(5)	1.467(7)
Pentagon (deg)		105.0(3)	103.0(4)
Pentagon (deg)		109.9(4)	107.1(2)
Pentagon (deg)		110.0(2)	111.4(4)
Hexagon (deg)		118.2(2)	117.7(3)
Hexagon (deg)		118.4(3)	119.2(4)
Hexagon (deg)		119.9(2)	120.4(2)
Hexagon (deg)		121.6(3)	120.8(4)
Hexagon (deg)		121.9(4)	121.9(2)

References

1. Zachariasen WH (1951) The crystal structure of plutonium sesquicarbide. Argonne National Laboratory report #ANL-4631, Chicago
2. Rietveld HM (1969) A profile refinement method for nuclear and magnetic structures. J Appl Crystallogr 2:65
3. Giacovazzo C (2002) Fundamentals of crystallography, 2nd edn. Oxford University Press, Oxford
4. Dinnebier RE, Billinge SJL (2008) Powder diffraction theory and practice. Royal Society of Chemistry, Cambridge
5. Caglioti G, Paoletti A, Ricci RP (1958) Choice of collimators for a crystal spectrometer for neutron diffraction. Nucl Instrum 3:223–228
6. Klug HP, Alexander LE (1974) X-ray diffraction procedures for polycrystalline and amorphous materials. Wiley, New York
7. Cheary RW, Coelho AA (1992) A fundamental parameters approach to x-ray line-profile fitting. J Appl Crystallogr 25:109
8. Larsen AC, Von Dreele RB (1985) GSAS: General Structure Analysis System, Los Alamos National Laboratory report MS-H805. Los Alamos, New Mexico
9. McCusker LB, Von Dreele RB, Cox DE, Louër D, Scardi P (1999) Rietveld refinement guidelines. J Appl Crystallogr 32:36
10. Toby BH (2006) R factors in Rietveld analysis: how good is good enough? Powder Diffr 21:67
11. Buchsbaum C, Schmidt MU (2007) Rietveld refinement of a wrong crystal structure. Acta Crystallogr B 63:926
12. Le Bail A (2005) Whole powder pattern decomposition methods and applications: a retrospection. Powder Diffr 20:316–326
13. Pawley GS (1981) Unit-cell refinement from powder diffraction scans. J Appl Crystallogr 14:357–361
14. David WIF, Shankland K, Shankland N (1998) Routine determination of molecular crystal structures from powder diffraction data. Chem Commun 8:931–932

15. David WIF (2004) On the equivalence of the Rietveld method and the correlated integrated intensities method in powder diffraction. J Appl Crystallogr B 37:621
16. Pagola S et al (2010) The structure of malaria pigment β-hematin. Nature 404:307; Pagola S, Stephens PW (2010) PSSP, a computer program for the crystal structure solution of molecular materials from X-ray powder diffraction data. J Appl Crystallogr 43:370–376
17. Huq A, Stephens P (2005) Transition temperatures and vacancies in superconducting Rb3C60. Phys Rev B 72:092511
18. Stephens PW (1999) Phenomenological model of anisotropic peak broadening in powder diffraction. J Appl Crystallogr 32:281; Stokes AR, Wilson AJC (1944) The diffraction of x-rays by distorted crystal aggregates. Proc Phys Soc Lond 56:174
19. Bruker AXS (2005) Topas V3: general profile and structure analysis software for powder diffraction data – user's manual; Bruker AXS, Karlsruhe; Coehlo AA (2007) TOPAS academic. Coelho Software, Brisbane. http://www.topas-academic.net